
[View Journal Online](#)  
[View Article Online](#)

# Synthesis and structural characterization and DFT calculations of the organic salt crystal obtaining 9-aminoacridine and picric acid: 9-Aminoacridinium picrate

 Fatma Aydın <sup>1,\*</sup> and Nahide Burcu Arslan <sup>2</sup>
<sup>1</sup> Department of Chemistry, Sciences Faculty, Çanakkale Onsekiz Mart University, 17100, Çanakkale, Turkey

<sup>2</sup> Department of Computer Education and Instructional Technology, Faculty of Education, Giresun University, 28200, Giresun, Turkey

 \* Corresponding author at: Department of Chemistry, Sciences Faculty, Çanakkale Onsekiz Mart University, 17100, Çanakkale, Turkey.  
 e-mail: [faydin@comu.edu.tr](mailto:faydin@comu.edu.tr) (F. Aydın).

## RESEARCH ARTICLE



doi 10.5155/eurjchem.14.3.376-384.2462

 Received: 15 June 2023  
 Received in revised form: 17 July 2023  
 Accepted: 26 July 2023  
 Published online: 30 September 2023  
 Printed: 30 September 2023

## KEYWORDS

 Picric acid  
 Thermal stability  
 Frontier molecular orbitals  
 9-Aminoacridinium picrate  
 X-ray structure determination  
 Molecular electrostatic potential

## ABSTRACT

Organic salt, 9-aminoacridinium picrate (9-AAcPc), containing equimolar quantities of 9-aminoacridine and picric acid was obtained and a single crystal was grown by the slow evaporation method in the mixture of methanol: tetrahydrofuran solvent (1: 1, v: v). The molecular structure of the prepared compound was confirmed by FT-IR, <sup>1</sup>H NMR, and <sup>13</sup>C NMR spectroscopic methods, as well as single crystal X-ray diffraction analysis. The X-ray diffraction analysis of the crystal structure of the title compound showed the presence of the triclinic space group *P*-1 with no. 2, *a* = 8.2811(7) Å, *b* = 10.1003(9) Å, *c* = 13.4484(13) Å,  $\alpha$  = 83.521(3)°,  $\beta$  = 83.330(3)°,  $\gamma$  = 66.595(3)°, *V* = 1022.56(16) Å<sup>3</sup>, *Z* = 2,  $\mu$ (MoK $\alpha$ ) = 0.108 mm<sup>-1</sup>, *D*<sub>calc</sub> = 1.375 g/cm<sup>3</sup>, 56338 reflections measured (5.89° ≤ 2 $\theta$  ≤ 56.704°), 5097 unique (*R*<sub>int</sub> = 0.0400, *R*<sub>sigma</sub> = 0.0210) which were used in all calculations. The final *R*<sub>1</sub> was 0.0552 (*I* > 2 $\sigma$ (*I*)) and *wR*<sub>2</sub> was 0.1757 (all data). The molecular geometry was also optimized using density functional theory. The frontier molecular orbitals were calculated, and we discussed the probability that the proton transfers from the phenolic OH group of picric acid to different nitrogen units. The calculated electronic structure properties of the title molecule, such as the HOMO and LUMO analysis, and different molecular electrostatic potential maps, were obtained by using the density functional theory method, and the calculated structure was compared with the experimental structure. The thermal stability of the crystal was also analyzed using the TGA/DTG technique.

 Cite this: *Eur. J. Chem.* 2023, 14(3), 376-384

 Journal website: [www.eurjchem.com](http://www.eurjchem.com)

## 1. Introduction

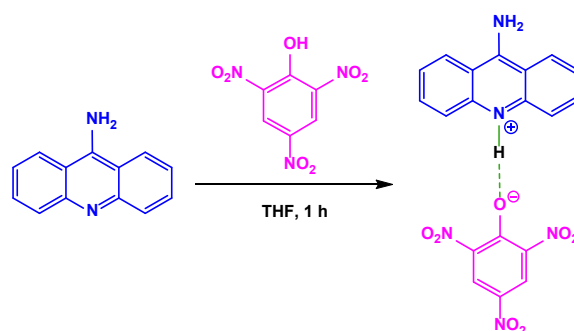
9-Aminoacridine (9-AAc) is a structurally polycyclic aromatic amine compound in which aniline and pyridine units are fused [1]. It is bright yellow in color and is one of the important dyestuffs with high fluorescence properties used in industry and medical applications [2-6]. In addition, the 9-aminoacridine molecule is seen to be used as matrix-assisted laser desorption/ionization (MALDI) material for some low-molecule weight compounds [7]. It is a promising material for use in optical and optoelectronic applications [8]. In addition to these applications, it is the subject of research in the fields of biology and medicine, as it is a structure with antibacterial and mutation activity [9,10]. For example, its applications in antitumor drugs are being studied in terms of its ability to bind to structures such as DNA [11-14].

Both pyridine and aniline have a nitrogen atom in their structure, while 9-aminoacridine, a polycyclic aromatic amine, has two different nitrogen atoms and each of the nitrogen contains a lone pair of electrons. In the case of aniline, the lone pair of electrons on the nitrogen atom accompanies the resonance with the  $\pi$  electron of the aromatic ring. Thus, the availability of electrons for donation is not easy, which decreases the

tendency to donate electrons, and hence the basicity of aniline decreases. In addition, in the case of pyridine, the lone electron on the nitrogen atom does not participate in the resonance, since the *p* orbitals of the aromatic carbon atoms are mutually perpendicular to the *p* orbital of the nitrogen atom. Therefore, it is known that the basicity of pyridine is greater than that of aniline, since the lone electron pair in the nitrogen atom can easily be donated to the electron-deficient element, ion or group [15]. Similar properties are expected to be observed in the structure as 9-aminoacridine, where aniline and pyridine unit fuse.

On the one hand, 2,4,6-trinitrophenol (picric acid, PA) is a phenol derivative containing three nitro groups and is truly one of the strongest organic acids (*pK*<sub>a</sub> = 0.38) [16]. Picric acid is extensively used for many purposes in manufacturing, pharmaceuticals, agriculture, etc. [17]. Furthermore, picric acid is one of the nonlinear organic materials (NLO) that can act as an acidic ligand, because it tends to form salts, particularly with aromatic or aliphatic amines [18-21].

In this study, an organic salt named 9-aminoacridinium picrate was synthesized (Scheme 1) and its single crystal was grown using the slow solvent evaporation technique. Its molecular structure was characterized by elemental analysis,



**Scheme 1.** The synthesis of the 9-AAcPc crystal.

FT-IR,  $^1\text{H}$  NMR, and  $^{13}\text{C}$  NMR spectroscopic techniques. The hydrogen bond geometry of the molecule was determined by the single-crystal X-ray diffraction technique. The transfer of a phenolic proton to a possible amine unit was investigated experimentally and theoretically. In addition, the properties of structural geometry, molecular electrostatic potential maps (MEP), and frontier molecular orbitals (FMO: The highest occupied molecular orbital (HOMO) and the lowest unoccupied molecular orbital (LUMO)) for the two probably structures were obtained by calculations based on the density functional theory (DFT)/B3LYP method with 6-311G basis set and the FMO's energy-correlated properties were interpreted for them. The thermal stability of the crystal was also analyzed by thermogravimetric analysis/differential thermogravimetric analysis/derivative thermal analysis (TGA/DTG/DTA) technique, and some thermodynamic parameters were calculated.

## 2. Experimental

### 2.1. General remarks

Reagents such as picric acid, 9-aminoacridine, and solvents were purchased from Sigma-Aldrich and solvents were used without purification. The melting point was measured on an Electro Thermal IA 9100 apparatus using a capillary tube and is uncorrected. A PerkinElmer Fourier Transform-Infrared (BX 100 FT-IR) spectrometer equipped with an ATR device was used to confirm the structure and the IR spectrum was recorded in the range 4000-650  $\text{cm}^{-1}$ . The  $^1\text{H}$  NMR and  $^{13}\text{C}$  NMR spectra were obtained on a JEOL ECX-400 NMR spectrometer operating at 400 and 100 MHz, respectively, using  $\text{DMSO-}d_6$  as solvent. The thermal behavior of the title compound was investigated by using PerkinElmer Pyris Sapphire thermogravimetric analysis (TGA) under nitrogen atmosphere. TGA measurement was carried out with a heating rate of 10  $^\circ\text{C}/\text{min}$  in the range of 20 to 1000  $^\circ\text{C}$ .

### 2.2. The synthesis of the 9-aminoacridinium picrate (9-AAcPc)

Picric acid (1 wt. % in  $\text{H}_2\text{O}$ ) was dried for two days at room temperature and recrystallized in ethanol. Crystallized picric acid (1.145 g, 5 mmol) was dissolved in dry tetrahydrofuran (10 mL) and 9-aminoacridine (0.971 g, 5 mmol) in THF (10 mL) was added dropwise to the above solution. This mixture was refluxed with stirring for 1 h. The yellow precipitate was then filtered using Whatman filter paper and dried in a vacuum desiccator. The resulting picrate salt crystals were grown by the slow evaporation method in the methanol/tetrahydrofuran mixed solvent (1:1, v:v). Yield: 90.7%. M.p.: 281-282  $^\circ\text{C}$ . FT-IR (ATR, v,  $\text{cm}^{-1}$ ): 3470, 3384, 3283, 3163, 3014, 1692, 1658, 1622, 1546, 1475, 1317, 1263, 1160, 905, 744.  $^1\text{H}$  NMR (400 MHz,  $\text{DMSO-}d_6$ ,  $\delta$ , ppm): 9.88 (br, 2H,  $\text{NH}_2$ ), 8.49 (s, 2H, Pic-H), 8.57 (d, 2H, Ar-H), 7.79 (d, 2H, Ar-H), 7.97 (t, 2H, Ar-H), 7.57 (t, 2H,

Ar-H).  $^{13}\text{C}$  NMR (100 MHz,  $\text{DMSO-}d_6$ ,  $\delta$ , ppm): 161.3 (C15), 158.3 (C13), 142.2 (C14, C16), 139.7 (C6, C7), 136.1 (C4, C9), 125.7 (C3, C10), 125.1 (C17, C19), 124.6 (C18), 124.3 (C2, C11), 119.2 (C5, C8) and 112.0 (C1, C12).

### 2.3. Crystallography

The unit cell parameters and crystal structure of 9-AAcPc were determined from single crystal X-ray diffraction data. A yellow crystal with a dimension of 0.13  $\times$  0.12  $\times$  0.10 mm was selected for data collection that was performed on a Bruker APEX-II CCD automatic diffractometer with graphite-monochromatized Mo-K $\alpha$  radiation ( $\lambda = 0.71073 \text{ \AA}$ ) using the  $\phi$  and  $\omega$ -scan mode at 296 K. The crystal structure was solved and refined by the SHELXS-97 and SHELXL-97 programs implemented in the WinGX [22] program suite, respectively [23,24]. The refinement was carried out by the full-matrix least-squares method on the positional and anisotropic temperature parameters of the non-hydrogen atoms, or equivalently, corresponding to 300 crystallographic parameters. All non-hydrogen atoms were refined anisotropically, whereas hydrogen atoms were located geometrically and refined as riding with respective C-H distances of 0.93  $\text{Å}$  corresponding to the aromatic C-H bonds. The atomic numbering scheme with displacement ellipsoids of the crystal structure drawn with ORTEP III [22] was depicted at the 30% probability level for clarity (Figure 1). The general-purpose crystallographic tool PLATON was used for the structure analysis and presentation of the results [25]. Details of the data collection conditions and the parameters of the compound refinement process are given in Table 1.

In the title compound, there is a disordered tetrahydrofuran molecule with very large displacement parameters, which could not be properly modeled. The diffused electron density resulting from this was removed by the SQUEEZE routine in PLATON [25]. There is one cavity of volume 124  $\text{Å}^3$  per unit cell centered at (0, 0, 0). This cavity contains approximately 40 electrons which were assigned to one solvent tetrahydrofuran molecule. Since Z is equal to 2, each salt compound has 0.5 solvent tetrahydrofuran equivalent. In the final refinement, this contribution was removed from the intensity data to produce better refinement results. Additionally, atoms O4 and O5 were disordered over two positions, and the refined site occupancy factors of the disordered atoms are 0.783(5)% for the major position and 0.217(5)% for the minor position, respectively.

## 3. Results and discussion

### 3.1. Description of the crystal structure and optimized geometry

The good quality crystals of 9-aminoacridinium picrate (9-AAcPc) were synthesized and grown by the slow evaporation method.

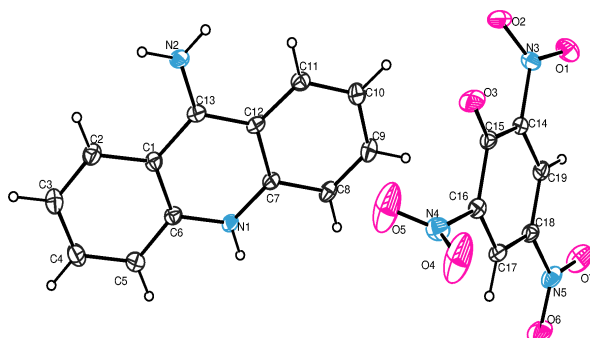
**Table 1.** Crystal data and structure refinement parameters for 9-AAcPc.

Empirical formula	C <sub>19</sub> H <sub>13</sub> N <sub>5</sub> O <sub>7</sub>
Formula weight (g/mol)	423.34
Temperature (K)	296.15
Crystal system	Triclinic
Space group	<i>P</i> -1
<i>a</i> , (Å)	8.2811(7)
<i>b</i> , (Å)	10.1003(9)
<i>c</i> , (Å)	13.4484(13)
$\alpha$ (°)	83.521(3)
$\beta$ (°)	83.330(3)
$\gamma$ (°)	66.595(3)
Volume (Å <sup>3</sup> )	1022.56(16)
<i>Z</i>	2
$\rho_{\text{calc}}$ (g/cm <sup>3</sup> )	1.375
$\mu$ (mm <sup>-1</sup> )	0.108
<i>F</i> (000)	436.0
Crystal size (mm <sup>3</sup> )	0.13 × 0.12 × 0.1
Radiation	MoK $\alpha$ ( $\lambda$ = 0.71073)
2 $\theta$ range for data collection (°)	5.89 to 56.704
Index ranges	-11 ≤ <i>h</i> ≤ 11, -13 ≤ <i>k</i> ≤ 13, -17 ≤ <i>l</i> ≤ 17
Reflections collected	56338
Independent reflections	5097 [R <sub>int</sub> = 0.0400, R <sub>sigma</sub> = 0.0210]
Data/restraints/parameters	5097/50/300
Goodness-of-fit on <i>F</i> <sup>2</sup>	1.048
Final <i>R</i> indexes [I ≥ 2 $\sigma$ (I)]	R <sub>1</sub> = 0.0552, wR <sub>2</sub> = 0.1549
Final <i>R</i> indexes [all data]	R <sub>1</sub> = 0.0767, wR <sub>2</sub> = 0.1757
Largest diff. peak/hole (e.Å <sup>-3</sup> )	0.56/-0.34

**Table 2.** Geometric details of intramolecular hydrogen bonding for 9-AAcPc crystal (Å, °).

D—H...A	D—H	H...A	D...A	$\angle$ D—H...A
N1—H1...O3 <sup>i</sup>	0.86	1.86	2.721 (3)	174
N2—H2...O2 <sup>ii</sup>	0.86	2.306	3.088	151

Symmetry code: (i) *x*+1, *y*, *z*; (ii) *-x*+1, *-y*+1, *-z*+1

**Figure 1.** ORTEP III diagram of the 9-AAcPc crystal.

The cell parameters and crystallographic planes were confirmed by single-crystal XRD analysis. The compound crystallizes as a yellow prism shaped in the triclinic system, space group *P*-1 with cell constants: *a* = 8.2811(7) Å, *b* = 10.1003(9) Å, *c* = 13.4484(13) Å,  $\alpha$  = 83.521 (3)°  $\beta$  = 83.330 (3)°  $\gamma$  = 66.595 (3)°, *V* = 1022.56 (16) Å<sup>3</sup>, *Z* = 2. In the title compound, 9-AAcPc, one of the nitro groups of the picrate moiety lies in the plane of the attached benzene ring (dihedral angle = 2.9°) while the other two are twisted by 19° and 120°. In addition, the 9-aminoacridinium moiety is planar, the maximum deviation from the mean plane belongs to the C9 atom with 0.02 Å. In the title crystal, two N—H...O type intermolecular hydrogen bonds are observed, Table 2. As expected, intermolecular hydrogen bonds occur between the N—H atoms of the 9-aminoacridinium moiety and the oxygen atoms of the picrate moiety (Figure 2). The first is between the N—H of the 9-aminoacridinium moieties and the O3 atom of the picrate moieties with donor acceptor distance 2.721 Å and symmetry code (*x*+1, *y*, *z*). Similarly, the other is between one of the hydrogens of NH<sub>2</sub> in the 9-aminoacridinium moieties and O2 in the picrate moieties with the donor acceptor distance 3.088 Å and the symmetry code (*-x*+1, *-y*+1, *-z*+1).

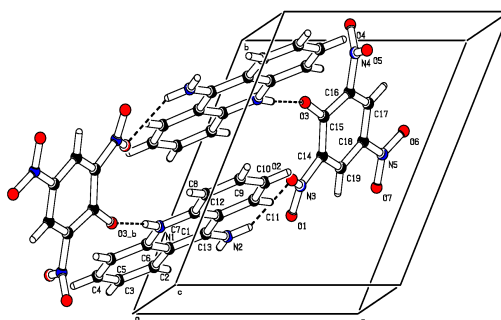
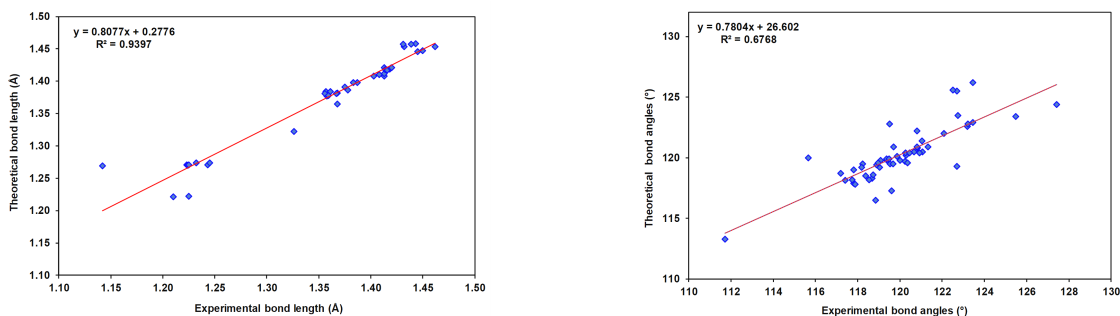
The optimized geometric parameters (theoretical), namely, the bond lengths, bond angles, and torsion angles calculated by the B3LYP/6-311G method corresponding to the experimental values (X-ray) for 9-AAcPc, are listed in Table 3. Correlation studies of the lengths and angles of the bonds obtained from Table 3 are shown in Figure 3. The correlation coefficients (*r*) between these parameters were calculated as 0.9694 and 0.8227 for the bond length and bond angles, respectively. Figure 3 revealed that all optimized parameters were generally slightly different from the experimental values. Here, the experimental values are defined to be in the solid phase, and the theoretical calculations are in the gas phase. In the solid state, molecules have connected with together due to intermolecular interactions in the unit cell during crystal formation, which result in the differences in parameters between the calculated and experimental values [26].

### 3.2. Powder X-ray diffraction

The XRD method is widely used for the detection of polymorphisms and is a useful tool to judge the phase purity of the single crystal. To investigate the crystal structure and crystallinity of the 9-aminoacridinium picrate, XRD measurements of single crystal and powder were made.

**Table 3.** The experimental and optimized geometric parameters (bond length (Å), bond angle (°)) of the 9-AAcPc, obtained by B3LYP/6-311G density functional calculation in the gas phase.

Bond lengths (Å)			Bond lengths (Å)		
	X-ray	B3LYP		X-ray	B3LYP
N1—C6	1.357(2)	1.384	C3—C4	1.403(3)	1.408
N1—C7	1.358(2)	1.377	C4—C5	1.361(3)	1.384
N2—C13	1.326(2)	1.322	C5—C6	1.413(2)	1.408
N3—O1	1.223(2)	1.271	C7—C8	1.413(2)	1.412
N3—O2	1.232(2)	1.274	C7—C12	1.414 (2)	1.418
N3—C14	1.445(2)	1.446	C8—C9	1.356 (3)	1.381
N4—O4A	1.142(3)	1.269	C9—C10	1.408(3)	1.410
N4—O5A	1.243(3)	1.271	C10—C11	1.367(3)	1.381
N4—C16	1.462(2)	1.453	C11—C12	1.416(2)	1.417
N5—O7	1.224(2)	1.270	C12—C13	1.431(2)	1.457
N5—O6	1.225(2)	1.271	C14—C19	1.378(2)	1.386
N5—C18	1.450(2)	1.447	C14—C15	1.443(2)	1.458
O3—C15	1.2451(19)	1.274	C15—C16	1.439(2)	1.457
C1—C6	1.413(2)	1.421	C16—C17	1.359(2)	1.378
C1—C2	1.418(2)	1.419	C17—C18	1.387(2)	1.398
C1—C13	1.432(2)	1.453	C18—C19	1.375(2)	1.391
C2—C3	1.368(3)	1.382			
Bond angles (°)			Bond angles (°)		
	X-ray	B3LYP		X-ray	B3LYP
C6—N1—C7	122.70(13)	125.5	C8—C9—C10	120.92(16)	120.4
O1—N3—O2	122.08(16)	122.0	C11—C10—C9	120.01(17)	119.8
O1—N3—C14	119.53(16)	119.5	C10—C11—C12	121.04(16)	121.4
O2—N3—C14	118.39(16)	118.5	C7—C12—C11	117.88(14)	117.8
O4A—N4—O5A	119.5(3)	122.8	C7—C12—C13	118.90(14)	119.4
O4A—N4—C16	122.7(2)	119.3	C11—C12—C13	123.21(14)	122.8
O5A—N4—C16	117.81(18)	117.9	N2—C13—C12	120.45(15)	120.4
O7—N5—O6	122.75(17)	123.5	N2—C13—C1	120.81(15)	120.9
O7—N5—C18	118.69(17)	118.3	C12—C13—C1	118.73(13)	118.6
O6—N5—C18	118.55(17)	118.2	C19—C14—C15	123.45(14)	122.9
C6—C1—C2	117.75(16)	118.2	C19—C14—N3	123.45(14)	126.2
C6—C1—C13	119.05(14)	119.2	C15—C14—N3	119.71(14)	120.9
C2—C1—C13	123.19(15)	122.6	O3—C15—C16	120.82(16)	122.2
C3—C2—C1	120.84(17)	120.8	O3—C15—C14	127.42(15)	124.4
C2—C3—C4	120.28(18)	120.2	C16—C15—C14	111.73(13)	113.3
C5—C4—C3	121.06(18)	120.5	C17—C16—C15	125.49(15)	123.4
C4—C5—C6	119.40(17)	119.8	C17—C16—N4	118.84(15)	116.5
N1—C6—C1	120.25(15)	119.7	C15—C16—N4	115.67(14)	120.0
N1—C6—C5	119.09(14)	119.8	C16—C17—C18	118.23(15)	119.5
C1—C6—C5	120.66(15)	120.5	C19—C18—C17	121.34(14)	120.9
N1—C7—C8	119.38(14)	119.9	C19—C18—N5	118.98(16)	119.6
N1—C7—C12	120.35(14)	119.6	C17—C18—N5	119.68(15)	119.5
C8—C7—C12	120.26(15)	120.4	C18—C19—C14	119.49(15)	119.9
C9—C8—C7	119.87(15)	120.1			

**Figure 2.** Molecular packing diagram displaced along the  $a$ -axis, geometric dimer structure of the 9-AAcPc.**Figure 3.** Correlation studies of calculated and experimental bond lengths and bond angles of the 9-AAcPc.

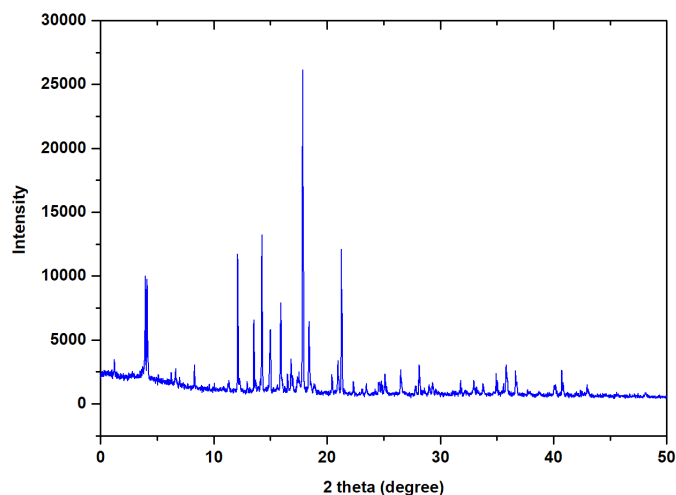


Figure 4. Powder X-ray diffraction spectrum for 9-AAcPc.

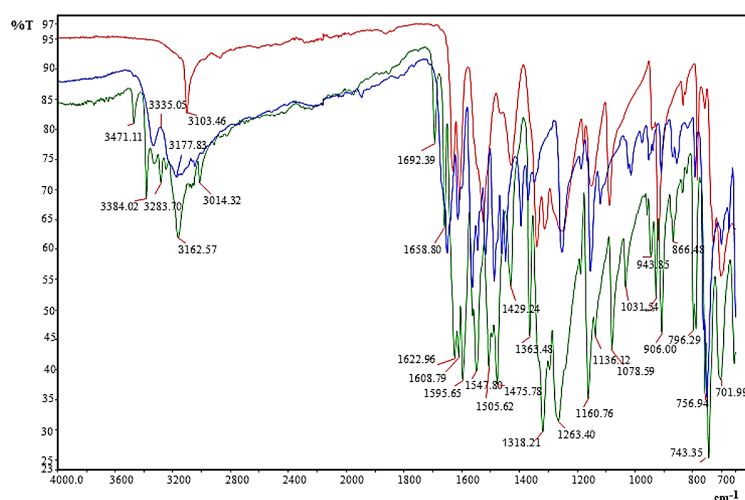


Figure 5. The FT-IR spectra of the 9-AAcPc (green), 9-aminoacridine (blue), and picric acid (red).

The title crystal was subjected to a powder X-ray diffraction study using a PANalytical Empyrean diffractometer with Cu-K $\alpha$  ( $\lambda = 1.5406 \text{ \AA}$ ) radiation and the crystalline structure of the 9-AAcPc compound was determined by solving the sharp and well defined Bragg peaks using the XRDA software [27]. Figure 4 shows that the 9-AAcPc crystal has a high phase purity.

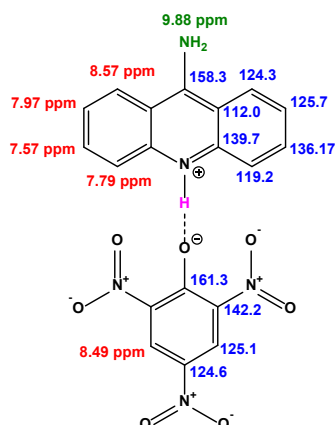
### 3.3. FT-IR spectral analysis

The vibrational frequencies of the functional groups in the crystal lattice of molecules of 9-AAcPc (red colour) and picric acid (green colour) and 9-aminoacridine (blue colour) molecules were characterized by the FT-IR spectrum as shown in Figure 5. Charge transfer complexes are formed by the interaction of an electron acceptor and the other is an electron donor [28,29]. Some of that is also explained as an acid-base interaction, which is the transfer of protons from the donor (Lewis acid) to the acceptor (Lewis base). It is known that some organic compounds easily form charge transfer complexes [30]. The formation of a charge transfer complex by the acceptor (9-aminoacridine) and donor (picric acid) molecules is strongly demonstrated by the data in the spectrum. As it can be seen from the spectrum, it is observed that the bands of the donor are slightly shifted to lower frequency and that of the acceptor are slightly shifted to higher frequency. This shift has been attributed to the charge transfer from the donor to the acceptor upon complexation. The band observed at  $3470 \text{ cm}^{-1}$  is assigned

to the N<sup>+</sup>-H stretching vibration due to the intermolecular hydrogen bonding (N<sup>+</sup>-H...O). The absorption band at  $3384 \text{ cm}^{-1}$  is due to the asymmetric N-H stretching vibration, while a weak absorption band observed at  $3332 \text{ cm}^{-1}$  is interoperated as a symmetric N-H stretching vibration. The aromatic C-H stretching vibrations appear at  $3283$ ,  $3163$ , and  $3014 \text{ cm}^{-1}$ . The C-H in-plane bending vibration was confirmed with a frequency of  $1078 \text{ cm}^{-1}$ . The aromatic C=C stretching vibration is exhibited at  $1605 \text{ cm}^{-1}$ . The peak of  $1160 \text{ cm}^{-1}$  is assigned to the C-NO<sub>2</sub> stretching vibration. The peaks at  $1547$  and  $1318 \text{ cm}^{-1}$  are due to symmetric and asymmetric NO<sub>2</sub> vibrations, respectively. The aromatic C-H out-of-plane bending vibration and the C-O stretching vibration bands appear at  $743$  and  $711 \text{ cm}^{-1}$  and  $1263 \text{ cm}^{-1}$ , respectively. The absorption bands observed at  $926$  and  $905 \text{ cm}^{-1}$  are explained by the NO<sub>2</sub> scissoring and wagging vibrations [31].

### 3.4. <sup>1</sup>H NMR and <sup>13</sup>C NMR spectral analysis

The picric acid phenolic hydroxyl proton signal, which is normally observed at  $\delta 11.94 \text{ ppm}$  [32], was not observed in the <sup>1</sup>H NMR spectrum as a result of proton migration to acridine nitrogen due to the formation of 9-AAcPc. The peaks that define the aromatic regions of the acridine and picrate moieties are seen as five signals in the spectrum. As an important criterion for the structural explanation of 9-AAcPc, the singlet peak at  $\delta 8.49 \text{ ppm}$  is assigned to the two protons at symmetrical *meta*



**Scheme 2.** The  $^1\text{H}$  NMR and  $^{13}\text{C}$  NMR chemical shifts of the 9-AAcPc in  $\text{DMSO-}d_6$ .

positions in the picrate moiety. Furthermore, the presence of broad peak  $\text{NH}_2$  protons with relative intensity  $\delta$  1.00 at 9.88 ppm and aromatic protons with relative intensities 1.00 at  $\delta$  8.57, 7.97, 7.79 and 7.55 ppm in the  $^1\text{H}$  NMR spectrum confirms the structure of 9-AAcPc. The 9-AAcPc magnetically and chemically consists of two different aromatic rings. The ipso carbon (C19) signal of the picrate moiety appears at  $\delta$  161.30 ppm. The weak peak signal at  $\delta$  158.35 ppm is assigned to the equivalent *ortho* carbons of the picrate moiety. The high intensity peaks at  $\delta$  142.21 and 139.72 ppm are due to the presence of magnetically and chemically carbons connected to nitrogen units of the acridinium moiety. Other aromatic carbons in the structure of 9-aminoacridinium picrate were confirmed around  $\delta$  136.17-112.00 ppm (Scheme 2).

### 3.5. The molecular orbital analysis

Molecular orbital theory is known as the theory of quantum chemistry, and the frontier molecular orbitals (FMOs), especially the highest occupied molecular orbital (HOMO) and the lowest unoccupied molecular orbital (LUMO), are two significant molecular orbitals as a result of the overlap of atomic orbitals. HOMO and LUMO have been widely used to understand the reactivity and region selectivity of various chemical systems. The narrower the energy gap of a molecule, the softer and more unstable the molecular structure, but the wider the HOMO and LUMO gap, the harder and more stable the molecular structure, and these soft molecules are chemically reactive and unstable [33]. Therefore, the HOMO and LUMO energy levels are essential energy levels to understand the chemical activity of a molecule. In molecular behavior, HOMO and LUMO are known as electron donor orbital and electron acceptor orbital, respectively [34]. The excitation energy is determined from the energy difference between the HOMO and LUMO energy eigenvalues. Molecular orbital energy values for two formulas (I and II), the total energies of the  $\text{C}_{19}\text{H}_{13}\text{N}_5\text{O}_7$  compounds were calculated using the B3LYP/6-311G method in the ground state, in the gas phase (Figure 6). Figure 6 shows the HOMO and LUMO plots of the complex salt as Formulas I and II. In formula I, HOMO is spread fully over the picrate moiety, while LUMO is spread entirely over the acridine ring. On the other hand, in the possible formula II structure, the HOMO is completely localized over the acridine ring, while the LUMO is completely spread over the picrate moiety.

The global reactivity parameters of the two forms were obtained using the molecular orbital energy values of  $\text{C}_{19}\text{H}_{13}\text{N}_5\text{O}_7$  (Table 4). The HOMO and LUMO energy levels are essential for understanding the chemical activity of a molecule. The narrower the HOMO and LUMO energy gap of a molecule, the softer and more unstable the molecular structure, but the

wider this energy gap, the harder and more stable the molecular structure [35]. The energy gap values of salt structures formed from 9-aminoacridine and picric acid are calculated as 3.3374 and 3.0928 eV for possible I and II, respectively. The larger energy gap value of the possible structure I, (3.3374 eV) indicates that this structure is more stable, and the single-crystal structure has also been confirmed. In addition to the lower value of chemical potential ( $\mu$ ), chemical hardness ( $\eta$ ) and global electrophilicity index ( $\omega$ ) from the global reactivity parameters of the molecular structure for the possible, I will explain the chemical reactivity properties.

### 3.6. Molecular electrostatic potential (MEP) analysis

The surface of the molecular electrostatic potential provides information about the partial molecular charges, the electronegativity of different atoms, and the regions of relative chemical reactivity for the investigated molecular structure. It is generally identified by the color classification scheme. Generally, the deep blue and red regions indicate the most electron-deficient and the most electron-rich regions or the positive and negative charge regions of the molecule, respectively. Furthermore, the green region represents the neutral region and the electrostatic potential increases in the order red < orange < yellow < green < blue colors on the surface [36]. The calculated MEP maps of Formulas I and II using the B3LYP/6-311G basis set and the scheme of possible crystal mechanisms are shown in Figure 7. From the MEP surface of Formula I (Figure 7, I), it can be seen that the minimum value ( $-9.602e^{-2}$ ) is located at the oxygen atoms of three nitro groups and the maximum value ( $9.602e^{-2}$ ) is located on the hydrogen atom of the  $\text{N}^+\text{-H}$  group of the fused pyridine moiety. On the other hand, from the MEP surface when the amino moiety of acridine is  $-\text{NH}_3^+$  (Figure 7, II), the maximum value of electron-deficient ( $9.154e^{-2}$ ) is found to be located at the three hydrogen atoms. Therefore, in Figure 7, we prove the existence of an intramolecular  $\text{N-H}\cdots\text{O}$  interaction hydrogen bond. The formula I structure is confirmed by supporting single crystal data, the formation of hydrogen bonds between the nitro group and the hydrogen atom of the amino group as a result of the electrostatic interaction of the picrate anion (Figure 2).

### 3.7. Thermal analysis

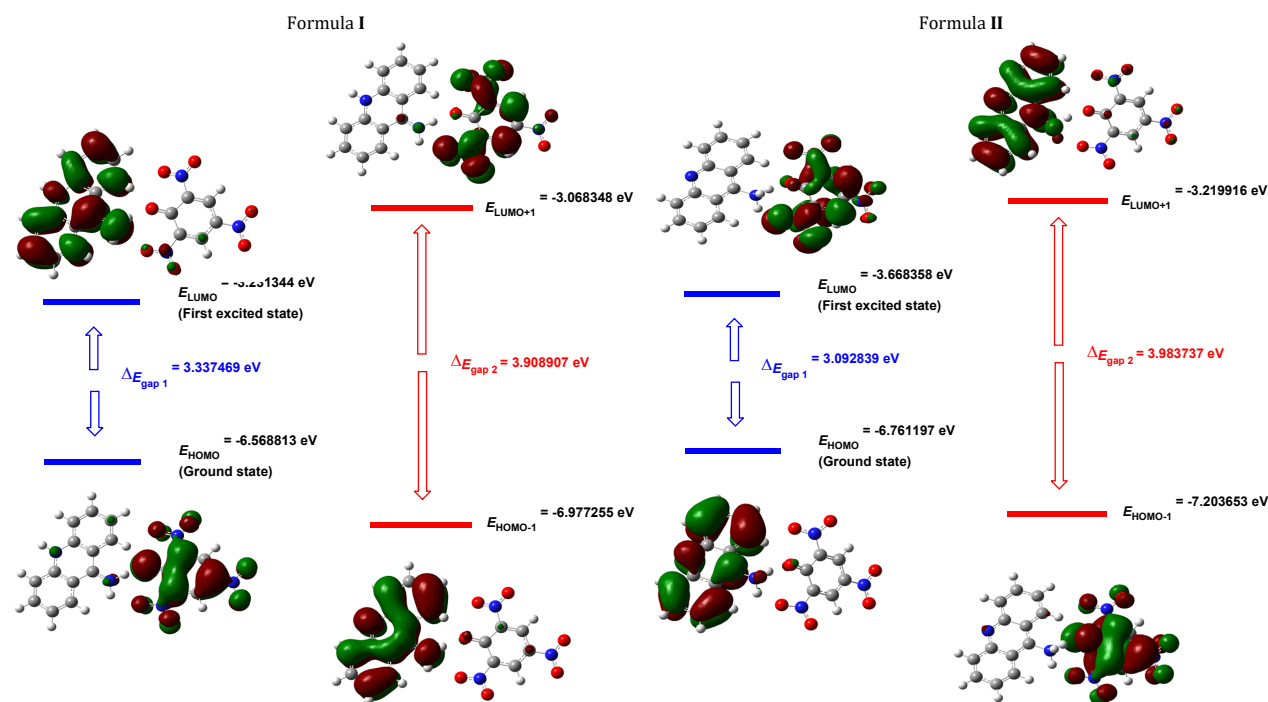
The TG/DTG/DTA curves of the 9-AAcPc crystal are depicted in Figure 8. In the DTA curve, the first peak at 142.56  $^\circ\text{C}$  is assigned to the dehydration of hygroscopic water (approximately 0.05%). After the dehydration of the hygroscopic water, the 9-AAcPc crystal undergoes two stages of decomposition.

**Table 4.** HOMO, LUMO and related global reactivity descriptor properties of the 9-aminoacridinium picrate (9-AAcPc) (I) and acridin-9-aminium picrate (II).

Molecular description, B3LYP/6-311G	9-Aminoacridinium picrate, I	Acridin-9-aminium picrate, II
Electronic Energy (a.u.)	-41683.5326	41682.4582
$E_{\text{HOMO}}$ (eV)	-6.5688	-6.7611
$E_{\text{LUMO}}$ (eV)	-3.2313	-3.6683
Ionization energy, $I = -E_{\text{HOMO}}$ (eV)	6.5688	6.7611
Electron affinity, $A = -E_{\text{LUMO}}$ (eV)	3.2313	3.6683
Energy band gap, $\Delta E = E_{\text{HOMO}} - E_{\text{LUMO}}$ (eV)	3.3375	3.0928
Chemical hardness, $\eta = (I - A) / 2$ (eV)	1.6687	1.5464
Chemical softness, $\zeta = 1/2\eta$ (eV)	0.2996	0.3233
Nucleophilicity, $\epsilon = 1/\omega$ (eV)	0.1389	0.1227
Chemical potential, $\mu = -(I + A) / 2$ (eV)	-4.9000	-5.2147
Electrophilicity index, $\omega = \mu^2 / 2\eta$ (eV)	7.1943	8.1479
Electronegativity, $\chi = (I + A) / 2$ (eV)	4.9000	5.2147
Dipol moment (Debye)	19.7858	10.8158

**Table 5.** Thermodynamic properties of 9-AAcPc at different temperatures at B3LYP/6-311G level.

T (K)	$C_{p,m}^0$ (cal.mol <sup>-1</sup> .K <sup>-1</sup> )	$S_m^0$ (cal.mol <sup>-1</sup> .K <sup>-1</sup> )	$\Delta H_m^0$ (kcal.mol <sup>-1</sup> )
100.00	40.808	109.688	2.718999
200.00	69.889	148.075	8.423688
298.15	99.615	182.353	16.94715
300.00	100.157	182.983	17.1354
400.00	127.282	216.193	28.74433
500.00	149.386	247.508	42.81937
600.00	166.751	276.707	58.86039
700.00	180.381	303.783	76.44258
800.00	191.228	328.869	95.24151
900.00	200.005	352.151	115.0168
1000.00	207.209	373.818	135.5879

**Figure 6.** Frontier molecular orbitals of the 9-aminoacridinium picrate (9-AAcPc) (I) and acridin-9-aminium picrate (II).

The DTA curve, which corresponds to the melting point of the 9-AAcPc crystal at 282.53 °C, shows a major endothermic peak, which is also present in the DTG curve. The second weight loss occurs at the temperature 321.13 °C and almost all compound decomposed are confirmed as its various gaseous products such as volatile substances, ammonia, and nitrogen dioxide gasses [37]. The second endothermic peak in the DTA curve shows that the compound is fully decomposed at 885.10 °C, as confirmed by the curve. This curve also shows that 9-AAcPc is stable up to 282.13 °C, and therefore this crystal can be used for several applications.

### 3.8. Thermodynamic properties

To understand the chemical stability of the molecular salt, thermodynamic properties are essential, which are obtained by the DFT method [38]. The values of some thermodynamic parameters such as enthalpy ( $\Delta H^\circ$ ), standard heat capacity of constant pressure ( $C_p^\circ$ ) and entropy ( $\Delta S^\circ$ ) for the 9-AAcPc crystal were calculated by DFT method with B3LYP/6-311G basis set for different temperatures 100-1000 K, in the 1 atm pressure and the scaled factor 0.961. The temperature dependence of the thermodynamic parameters such as enthalpy ( $\Delta H^\circ$ ), standard heat capacity of constant pressure ( $C_p^\circ$ ) and

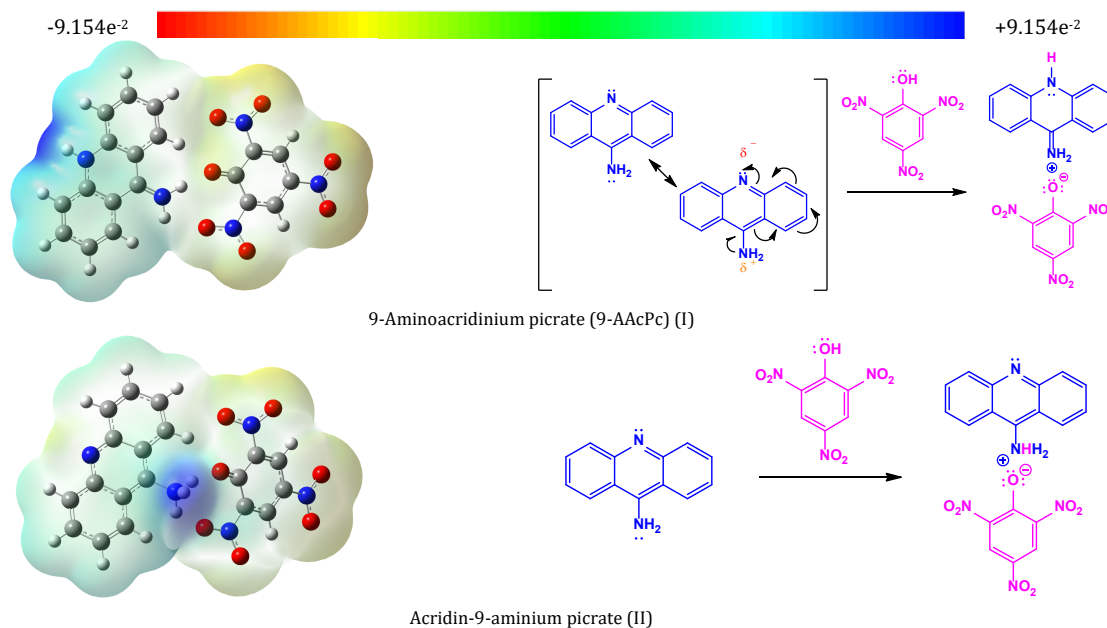


**Figure 7.** The MEP surfaces calculated by the DFT/B3LYP method and probably the crystal formulas of 9-aminoacridinium picrate (9-AAcPc) (I) and acridin-9-aminium picrate (II).

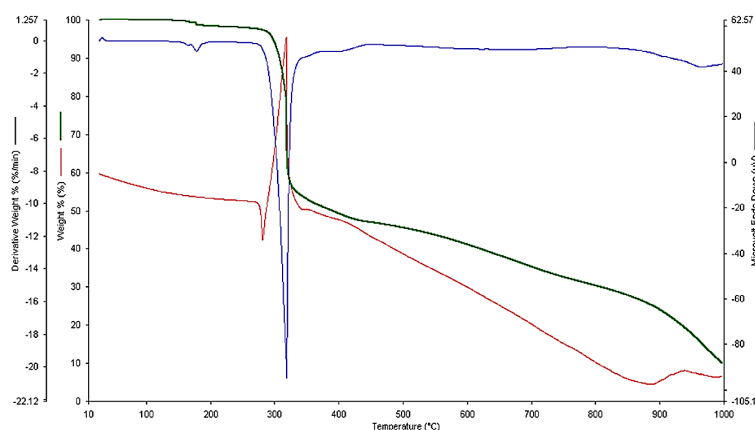


**Figure 8.** TGA-DTG-DTA thermograms of the 9-AAcPc crystal.

entropy ( $\Delta S^\circ$ ) of the title compound is given in Table 5, and the corresponding fitting equations are also given in Equations (1-3). As given in Table 5, all values are seen to increase when the temperature rises in the range of 100-1000 K, mainly because a higher temperature can strengthen the vibration of the title molecule.

$$C_{p,m}^\circ = 4.28895 + 0.37216 T - 1.70679 \times 10^{-4} T^2 \quad (1)$$

$(R^2 = 0.9993)$

$$S_m^\circ = 70.83131 + 0.40387 T - 1.01232 \times 10^{-4} T^2 \quad (2)$$

$(R^2 = 0.9999)$

$$\Delta H_m^0 = -5.00174 + 0.05004 T + 9.21101 \times 10^{-6} T^2 \quad (3)$$

$(R^2 = 0.9992)$

#### 4. Conclusions

A new salt of the organic charge transfer complex, 9-AAcPc, was synthesized and its single crystals were grown by a slow evaporation method using a mixture of methanol/ tetrahydrofuran (1:1, v:v). The molecular structure of 9-AAcPc was characterized by FT-IR,  $^1\text{H}$  and  $^{13}\text{C}$  NMR spectral techniques. The powder X-ray diffraction study confirms that the crystalline

perfection is fairly good. The single-crystal XRD study reveals that 9-AAcPc crystallizes in a triclinic crystal system with the *P*-1 space group. Experimental results and calculations determined that the complex salt consisting of a 9-aminoacridine and picric acid is 9-aminoacridinium picrate (Formula I), not the acridin-9-aminium picrate (Formula II) structure. Two N-H...O type intermolecular hydrogen bonds were observed in the crystal packing. The thermal behavior of 9-AAcPc was studied using TG-DTA and the crystal was stable up to 282 °C.

#### Acknowledgements

The financial support of the Çanakkale Onsekiz Mart University Grants Commission for a research grant (Project Number: 2016/672) was gratefully acknowledged.

#### CRedit authorship contribution statement

Conceptualization: Fatma Aydin; Methodology: Fatma Aydin, Nahide Burcu Arslan; Software: Nahide Burcu Arslan; Validation: Fatma Aydin; Formal Analysis: Nahide Burcu Arslan; Investigation: Fatma Aydin; Data Curation: Fatma Aydin, Nahide Burcu Arslan; Writing - Original Draft: Fatma Aydin; Writing - Review and Editing: Fatma Aydin, Nahide Burcu Arslan; Visualization: Fatma Aydin, Nahide Burcu Arslan; Project Administration: Fatma Aydin.

## Disclosure statement

Conflict of interests: The authors declare that they have no conflict of interest.  
Ethical approval: All ethical guidelines have been adhered.  
Sample availability: Sample of the compound is available from the authors.

## Supporting information

CCDC-2262891 contains the supplementary crystallographic data for the structure reported in this article. These data can be obtained free of charge via [http://www.ccdc.cam.ac.uk/data\\_request/cif](http://www.ccdc.cam.ac.uk/data_request/cif), by e-mailing [data\\_request@ccdc.cam.ac.uk](mailto:data_request@ccdc.cam.ac.uk) or by contacting The Cambridge Crystallographic Data Centre, 12, Union Road, Cambridge CB2 1EZ, UK; fax: +44-1223-336033.

## ORCID and Email

Fatma Aydin

 [faydin@comu.edu.tr](mailto:faydin@comu.edu.tr)

 <https://orcid.org/0000-0002-7219-6407>

Nahide Burcu Arslan

 [burcu.aslan@giresun.edu.tr](mailto:burcu.aslan@giresun.edu.tr)

 <https://orcid.org/0000-0002-1880-1047>

## References

- Morrin Acheson, R. *The chemistry of heterocyclic compounds, acridines*; John Wiley & Sons, 2009.
- Gellerman, G.; Gaisin, V.; Brider, T. One-pot derivatization of medicinally important 9-aminoacridines by reductive amination and SNAr reaction. *Tetrahedron Lett.* **2010**, *51*, 836–839.
- Stewart, J. T. Synthesis and Biological Activity of 9-substituted Acridines. *J. Pharm. Sci.* **1973**, *62*, 1357–1358.
- Sebestik, J.; Hlavacek, J.; Stibor, I. A role of the 9-aminoacridines and their conjugates in a life science. *Curr. Protein Pept. Sci.* **2007**, *8*, 471–483.
- Manivannan, C.; Renganathan, R. Spectroscopic investigation on the interaction of 9-Aminoacridine with certain dyes. *Spectrochim. Acta A Mol. Biomol. Spectrosc.* **2012**, *95*, 685–692.
- Maltman, B. A.; Dunsmore, C. J.; Couturier, S. C. M.; Tirnaveanu, A. E.; Delbederi, Z.; McMordie, R. A. S.; Naredo, G.; Ramage, R.; Cotton, G. 9-Aminoacridine peptide derivatives as versatile reporter systems for use in fluorescence lifetime assays. *Chem. Commun. (Camb.)* **2010**, *46*, 6929.
- Vermillion-Salsbury, R. L.; Hercules, D. M. 9-Aminoacridine as a matrix for negative mode matrix-assisted laser desorption/ionization. *Rapid Commun. Mass Spectrom.* **2002**, *16*, 1575–1581.
- Ahmed, S. A.; Obi-Egbedi, N. O.; Bamgbose, J. T.; Adeogun, A. I. Solvent enhancement of electronic intensity in acridine and 9-aminoacridine. *J. Saudi Chem. Soc.* **2016**, *20*, S286–S292.
- Stark, M. M.; Hall, N. C.; Nicholson, R. J.; Soelberg, K. 9-Aminoacridine, an effective antibacterial agent with caries-disclosing features. *Oral Surg. Oral Med. Oral Pathol.* **1968**, *26*, 560–562.
- Anikin, L.; Pestov, D. G. 9-aminoacridine inhibits ribosome biogenesis by targeting both transcription and processing of ribosomal RNA. *Int. J. Mol. Sci.* **2022**, *23*, 1260.
- Fornasiero, D.; Kurucsev, T. The binding of 9-aminoacridine to calf thymus DNA in aqueous solution electronic spectral studies. *Biophys. Chem.* **1985**, *23*, 31–37.
- Mangueira, V. M.; de Sousa, T. K. G.; Batista, T. M.; de Abrantes, R. A.; Moura, A. P. G.; Ferreira, R. C.; de Almeida, R. N.; Braga, R. M.; Leite, F. C.; Medeiros, K. C. de P.; Cavalcanti, M. A. T.; Moura, R. O.; Silvestre, G. F. G.; Batista, L. M.; Sobral, M. V. A 9-aminoacridine derivative induces growth inhibition of Ehrlich ascites carcinoma cells and antinociceptive effect in mice. *Front. Pharmacol.* **2022**, *13*.
- Chen, X.; Zhang, Y.; Chen, Y.; Zhang, J.; Chen, J.; Li, M.; Cao, W.; Chen, J. Synthesis and characterization of oxadisilole-fused 9-aminoacridines and 12-aminobenzo[b]acridines: Oxadisilole-fused 9-aminoacridines and 12-aminobenzo[b]acridines. *European J. Org. Chem.* **2014**, *2014*, 4170–4178.
- Su, T.-L.; Lin, Y.-W.; Chou, T.-C.; Zhang, X.; Bacherikov, V. A.; Chen, C.-H.; Liu, L. F.; Tsai, T.-J. Potent antitumor 9-anilinoacridines and acridines bearing an alkylating N-mustard residue on the acridine chromophore: Synthesis and biological activity. *J. Med. Chem.* **2006**, *49*, 3710–3718.
- Smith, M. B.; March, J. *March's advanced organic chemistry: Reactions, mechanisms, and structure*; 7th ed.; Wiley-Blackwell: Hoboken, NJ, 2012.
- CRC handbook of chemistry and physics*; Haynes, W. M., Ed.; 95th ed.; CRC Press: London, England, 2014.
- Ismail, M.; Khan, M. I.; Khan, S. B.; Akhtar, K.; Khan, M. A.; Asiri, A. M. Catalytic reduction of picric acid, nitrophenols and organic azo dyes via green synthesized plant supported Ag nanoparticles. *J. Mol. Liq.* **2018**, *268*, 87–101.
- Arslan, N. B.; Aydin, F. The crystal magnification, characterization, X-ray single crystal structure, thermal behavior, and computational studies of the 2,4,6-trimethylpyridinium picrate. *Eur. J. Chem.* **2022**, *13*, 468–477.
- Adam, A. M. A. Structural, thermal, morphological and biological studies of proton-transfer complexes formed from 4-aminoantipyrine with quinol and picric acid. *Spectrochim. Acta A Mol. Biomol. Spectrosc.* **2013**, *104*, 1–13.
- Stilinović, V.; Kaitner, B. Hydrogen bonding in pyridinium picrates: From discrete ion pairs to 3D networks. *Cryst. Growth Des.* **2011**, *11*, 4110–4119.
- Sethuram, M.; Bhargavi, G.; Rajasehakaran, M. V.; Dhandapani, M.; Amirthaganesan, G. Synthesis, crystal growth and characterisation of 2-aminomethylpyridinium picrate (2-amp)-a charge transfer molecular complex and organic nonlinear optical material. *Optik (Stuttg.)* **2014**, *125*, 55–60.
- Farrugia, L. J. *WinGX and ORTEP for Windows: an update.* *J. Appl. Crystallogr.* **2012**, *45*, 849–854.
- Sheldrick, G. M. SHELXL-97: Program for Crystal Structure Refinement, University of Gottingen, Germany, 1997.
- Sheldrick, G. M. SHELXS-97: Program for the Solution of Crystal Structures, University of Gottingen, Germany, 1997.
- Spek, A. L. Structure validation in chemical crystallography. *Acta Crystallogr. D Biol. Crystallogr.* **2009**, *65*, 148–155.
- Hoja, J.; Reilly, A. M.; Tkatchenko, A. First-principles modeling of molecular crystals: structures and stabilities, temperature and pressure: First-principles modeling of molecular crystals. *Wiley Interdiscip. Rev. Comput. Mol. Sci.* **2017**, *7*, e1294.
- Degen, T.; Sadki, M.; Bron, E.; König, U.; Nénert, G. The HighScore suite. *Powder Diffr.* **2014**, *29*, S13–S18.
- Bender, C. J. Theoretical models of charge-transfer complexes. *Chem. Soc. Rev.* **1986**, *15*, 475.
- Foster, R. *Organic Charge-transfer Complexes*; Academic Press: San Diego, CA, 1969.
- Nampally, V.; Palnati, M. K.; Baidla, N.; Varukolu, M.; Gangadhari, S.; Tigulla, P. Charge transfer complex between O-phenylenediamine and 2, 3-dichloro-5, 6-dicyano-1, 4-benzoquinone: Synthesis, spectrophotometric, characterization, computational analysis, and its biological applications. *ACS Omega* **2022**, *7*, 16689–16704.
- Smith, B. *Infrared spectral interpretation: A systematic approach*; CRC Press, 2018.
- Charisiadis, P.; Kontogianni, V.; Tsioufoulis, C.; Tzakos, A.; Siskos, M.; Gerotheranassis, I. 1H-NMR as a structural and analytical tool of intra- and intermolecular hydrogen bonds of phenol-containing natural products and model compounds. *Molecules* **2014**, *19*, 13643–13682.
- Pearson, R. G. Chemical hardness and density functional theory. *J. Chem. Sci. (Bangalore)* **2005**, *117*, 369–377.
- Brédas, J.-L. Organic electronics: Does a plot of the HOMO–LUMO wave functions provide useful information? *Chem. Mater.* **2017**, *29*, 477–478.
- Xu, Y.; Chu, Q.; Chen, D.; Fuentes, A. HOMO–LUMO gaps and molecular structures of polycyclic aromatic hydrocarbons in soot formation. *Front. Mech. Eng.* **2021**, *7*.
- Geerlings, P.; Proft, F. D.; Ayers, P. W. Chapter 1 Chemical reactivity and the shape function. In *Theoretical and Computational Chemistry*; Elsevier, 2007; pp. 1–17.
- Mageshwari, P. S. L.; Priya, R.; Krishnan, S.; Joseph, V.; Das, S. J. Growth, optical, thermal, mechanical and dielectric studies of sodium succinate hexahydrate ( $\beta$  phase) single crystal: A promising third order NLO material. *Opt. Laser Technol.* **2016**, *85*, 66–74.
- Bevan Ott, J.; Boerio-Goates, J. *Chemical Thermodynamics: Principles and applications*; 2000.



Copyright © 2023 by Authors. This work is published and licensed by Atlanta Publishing House LLC, Atlanta, GA, USA. The full terms of this license are available at <http://www.eurjchem.com/index.php/eurjchem/pages/view/terms> and incorporate the Creative Commons Attribution-Non Commercial (CC BY NC) (International, v4.0) License (<http://creativecommons.org/licenses/by-nc/4.0>). By accessing the work, you hereby accept the Terms. This is an open access article distributed under the terms and conditions of the CC BY NC License, which permits unrestricted non-commercial use, distribution, and reproduction in any medium, provided the original work is properly cited without any further permission from Atlanta Publishing House LLC (European Journal of Chemistry). No use, distribution, or reproduction is permitted which does not comply with these terms. Permissions for commercial use of this work beyond the scope of the License (<http://www.eurjchem.com/index.php/eurjchem/pages/view/terms>) are administered by Atlanta Publishing House LLC (European Journal of Chemistry).